University of Arkansas, Fayetteville

ScholarWorks@UARK

Detection of leukocytes stained with acridine orange using unique spectral features acquired from an image-based spectrometer

Courtney J. Hunter
University of Arkansas, Fayetteville

Follow this and additional works at: https://scholarworks.uark.edu/bmeguht

Part of the Bioimaging and Biomedical Optics Commons, Biomedical Devices and Instrumentation Commons, Cell Biology Commons, Computational Engineering Commons, Investigative Techniques Commons, and the Molecular, Cellular, and Tissue Engineering Commons

Citation

Detection of leukocytes stained with acridine orange using unique spectral features acquired from an image-based spectrometer

Senior Honors Thesis

by

Courtney J. Hunter

Department of Biomedical Engineering

College of Engineering

University of Arkansas

May 2017

Summary

A leukocyte differential count can be used to diagnosis a myriad blood disorders, such as infections, allergies, and efficacy of disease treatments. In recent years, attention has been focused on developing point-of-care (POC) systems to provide this test in global health settings. Acridine orange (AO) is an amphipathic, vital dye that intercalates leukocyte nucleic acids and acidic vesicles. It has been utilized by POC systems to identify the three main leukocyte subtypes: granulocytes, monocytes, and lymphocytes. Subtypes of leukocytes can be characterized using a fluorescence microscope, where the AO has a 450 nm excitation wavelength and has two peak emission wavelengths between 525 nm (green) and 650 nm (red), depending on the cellular content and concentration of AO in the cells. The full spectra of AO stained leukocytes has not been fully explored for POC applications. Optical instruments, such as a spectrometer that utilizes a diffraction grating, can give specific spectral data by separating polychromatic light into distinct wavelengths. The spectral data from this setup can be used to create object-specific emission profiles.

Yellow-green and crimson microspheres were used to model the emission peaks and profiles of AO stained leukocytes. Whole blood was collected via finger stick and stained with AO to gather preliminary leukocyte emission profiles. A MATLAB algorithm was designed to analyze the spectral data within the images acquired using the image-based spectrometer. The algorithm utilized watershed segmentation and centroid location functions to isolate independent spectra from an image. The output spectra represent the average line intensity profiles for each pixel across a slice of an object. First steps were also taken in processing video frames of manually translated microspheres. The high-speed frame rate allowed objects to appear in multiple consecutive images. A function was applied to each image cycle to identify repeating centroid locations.

The yellow-green (515 nm) and crimson (645 nm) microspheres exhibited a distinct separation in colorimetric emission with a peak-to-peak difference of 36 pixels, which is related to the 130 nm peak emission difference. Two AO stained leukocytes exhibited distinct spectral profiles and peaks across different wavelengths. This could be due to variations in the staining method (incubation period and concentration) effecting the emissions or variations in cellular content indicating different leukocyte subtypes. The algorithm was also effective when isolating unique centroids between video frames.

We have demonstrated the ability to extract spectral information from data acquired from the image-based spectrometer of microspheres, as a control, and AO stained leukocytes. We determined that the spectral information from yellow-green and crimson microspheres could be used to represent the wavelength range of AO stained leukocytes, thus providing a calibration tool. Also, preliminary spectral information was successfully extracted from yellow-green microspheres translated under the linear slit using stationary images and video frames, thus demonstrating the feasibility of collecting data from a large number of objects.
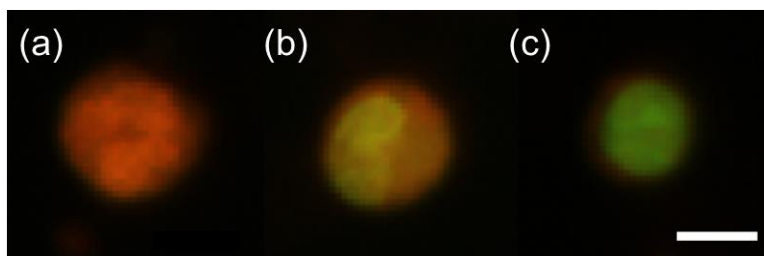
Introduction

Acridine orange (AO) is a fluorescent dye that was discovered by a group of botanists and later used in the fields of pathology and histology.[1] Early histological applications of AO were focused on the identification of malignant cells in tissue types such as cervical, endothelial, stomach, breast, and lung based on the unique fluorescent characteristics of the dye.[2] Also, research using AO was an attractive substitution to gram staining when identifying microbial, since AO was more sensitive and equally specific when compared to the traditional gram staining technique.[3] Originally, fluorescence-based AO staining techniques were performed on fixed monolayer of cells.[4] The individual cells can be characterized using a fluorescence microscope, where the AO has a 450 nm excitation wavelength and has two peak emission wavelengths between 525 nm (green) and 650 nm (red), depending on the cellular content and concentration of AO in the cells.[4,5] The staining of DNA in the nucleus of the malignant and microbial cells produced green fluorescence, while the RNA in the cytoplasm emitted a red-brown color.[2,6,7] An increased RNA concentration in the cells, characteristic of malignant cells, caused the cells to fluorescence, thus distinguishing them from healthy cells rich in DNA emitting green fluorescence.[2] However, these colorimetric distinctions were only applicable to early screenings of cell samples and could not be used as a true diagnostic tool, because the more established methods for diagnosis eliminated the doubt of colorimetric interpretation.[2]

The early biological applications of AO relied on the staining of fixed cells. Live cell staining with AO is more complex due to the ready uptake of the dye into the cells. The AO molecule is collected in the cell cytoplasm and is moved to the nucleus and acidic vesicles. The AO molecule initially intercalates into the DNA's major and minor grooves due to the amphipathic nature of the molecule.[8] If the cell possesses acidic vesicles, AO can be collected by the acidic vesicles, such as the lysosome, which has an internal pH of ~5 (4). The peak emission wavelength of AO in the cell is dependent on the uptake by the nucleic acids and acidic vesicles within the cell.[4,5]

AO has been used to stain and characterize leukocytes based on their varying nuclear and acidic vesicle concentrations across the five cellular subtypes: monocytes, lymphocytes, neutrophils, basophils, and eosinophils.[7,8] The neutrophils, basophils, and eosinophils are all classes of granulocytes. When AO is introduced to granulocytes, the molecule is collected and protonated in the acidic vesicles, preventing the molecule from passing back into the cytoplasm.[4,9] This

mechanism causes a high concentration of AO to be accumulated in these vesicles, thus causing the granulocytes to fluoresce red, **Figure 1-a**.[4,8,10] The lymphocytes have a low lysosome count and a largely dominant nucleus where the AO intercalates in the DNA, thus causing them to

Figure 1: The (a) granulocyte, (b) monocyte, and (c) lymphocyte exhibit distinct color features based on the concentrations of dye uptake in the acidic vesicles and nucleus. Scale bar 10 um. Image: Powless, A, et al. (8)

fluoresce green, **Figure 1-c**.[8,10] The monocytes exhibit an intermediate concentration of both DNA and acidic vesicles, so they fluoresce between the yellow and orange wavelengths, **Figure 1-b**.[8,10] This distinct colorimetric contrast between subtypes can be used to classify and count leukocyte populations based on colorimetric features alone.

A leukocyte differential is a clinical laboratory test that measures the concentrations of the subtypes of leukocytes. Fluctuations in the subtype concentrations can be used to diagnose a myriad of disorders, such as infections, allergies, and efficacy of disease treatments.[7] Currently, the "golden-standard" for leukocyte differential tests is an automated hematology analyzer, which classifies leukocytes based on electrical impedance and light scattering differences between the subtypes.[7,11] Although this method is time sensitive and reliable, it requires expensive equipment (≤$20,000) and reagents.[7] Earlier and lower cost methods of developing leukocyte counts can be performed manually by a trained technician, which is labor, skill, and time intensive.[12] These expensive or highly technical methods of leukocyte counting limit the accessibility and reliability of these tests in low income or remote areas.[7,12]

Point of care (POC) devices have been developed to aid in the skill and/or financial deficit when measuring leukocyte counts, thus increasing the availability of tests at a global health scale.[7,8] Three POC systems, in particular, have utilized AO staining as the contrast agent for a leukocyte differentials test.[7,8,13] These devices rely on the red-to-green emission intensity ratio, unique to the three main subtypes of leukocytes.[7,13] It is advantageous that these colorimetric differences can be distinguished with little pre-existing skill.[2] Another advantage of AO is its limited cell preparation (6-10 minutes) and imaging times (~3 minutes).[2,6] However, the AO fluorophore is unstable in daylight, has a limited imaging time due to photo bleaching and a significant

colorimetric shift.[4,5,6,8] The colorimetric shift occurs with variations in the staining method (incubation period and AO concentration), due to the accumulation of the dye by the cytoplasm and acidic vesicles.[8,9] Although AO has great potential to classify leukocytes for POC applications, the volatile nature of the dye can affect the reliability and accuracy of the test based on a ratio of AO emission intensity alone.

The full spectra of AO stained leukocytes has not been fully explored for POC applications. Optical instruments, such as a spectrometer that utilizes a diffraction grating, can give specific spectral data by separating polychromatic light into distinct wavelengths. A diffraction grating uses the concept of a multiple slit system to separate combined light into the individual color components.[14] The combination of the groove width and the change in refractive indices between the air and the glass of the grating causes the separation of light spectra when polychromatic light passes through the grating.[14] The grooves on the surface of the grating system determine the direction of the diffracted light. In particular, the direction is related to the wavelength of the transmitted light (λ), groove pitch (d), incidence angle (α) normal to the beam and diffraction angle (β), which can be related using the grating equation[15]:

$$m\lambda = d(sin\alpha + sin\beta).$$

Figure 2 depicts the scattering angles induced by the grating in response to a particular incident light. The variable m in the grating equation represents the diffraction order. The diffraction order describes the difference in spacing of the light depending on the wavelengths of light passing through the grooves.[15] The zero order (m = 0) represents the non-diffracted light because all wavelengths present are superimposed onto one another instead of separated.[15] The greater orders (m ≠ 0) represent diffraction depending on the magnitude of the respective wavelengths.[15] The resolution between wavelengths of light beams is referred to as the resolution of dispersion. Since the primary goal of using a diffraction grating, is to separate light into its individual
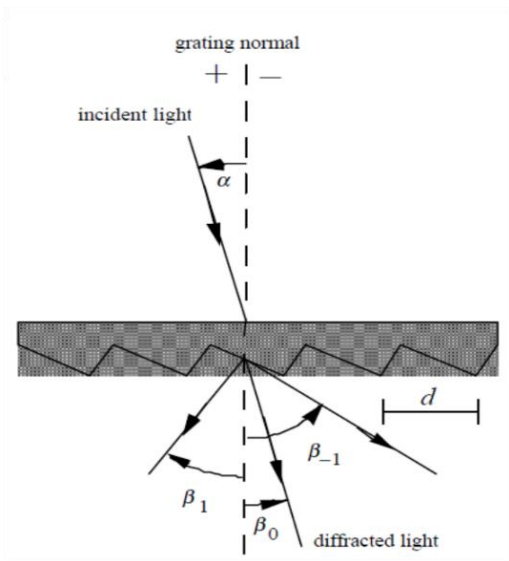
Figure 2: A schematic of the grating equation as it responds to the incident angle and the diffraction angles caused by the grooves. Image: Palmer, C, et al. (14)

color components, the resolution between color bands is dependent on the angular dispersion.[14] The angular dispersion is the angle range that the spectrum spreads per unit angle, so a greater angular dispersion results in a more distinct separation of the color bands.[14] The color bands produced by diffraction gratings are intensity-based; therefore, the intensity profile across the image produces the emission waveform (spectra) of the fluorophore being tested. Emission curves with distinct peaks that correspond to the different subtypes of AO stained leukocytes can be created based on the intensity-based profiles produced by these diffraction gratings.

The extracted spectra of whole objects consist of large data sets, and the spectra collected from many objects produce an unmanageable collection of information.   Technical computing software, such as MATLAB, can be used to analyze high volumes of information with minimal input from the user. We present a spectral extraction algorithm capable of extracting spectral information of fluorescent microspheres and AO stained cells obtained from images acquired via our image-based spectrometer.   Furthermore, the spectral data was collected from a small section of the object, which requires multiple spectral data to be combined.   Therefore, our algorithm includes a tracking method to distinguish different objects as the sample is translated under the system. The fluorescent microspheres were used to represent the range of emission wavelengths related to AO stained leukocytes. The results of this spectral information could be used to improve the reliability of AO as a method to classify leukocytes in a three-part differential test for POC applications.

Materials and Methods

I.   *Optical Configuration & Diffraction Grating Alignment*

The image-based spectrometer, **Figure 3**, comprises of a 450 nm laser (LS, FTEC2, Blue Sky Research, Milpitas, CA) that is focused onto a single mode fiber. The laser beam is expanded to 10 mm through a series of two lenses (BE). The expanded beam passes through a cylindrical lens (CL) to create a light sheet, which is reflected to the 20X/0.50 NA objective (Nikon, USA) by a dichroic mirror (DM) with a cutoff of 475 nm. The sample emitted light is transmitted back through the objective (OBJ) and through a long pass filter (500 nm, Thorlabs, Newton, NJ). Then, the light passes through a 100 mm lens, which focuses the beam through a vertical adjustable width slit (AS, Newport, CA, USA) to minimize out of focus light. The thin linear light expands onto a 30 mm lens, which focuses the light onto the visible transmission diffraction

5
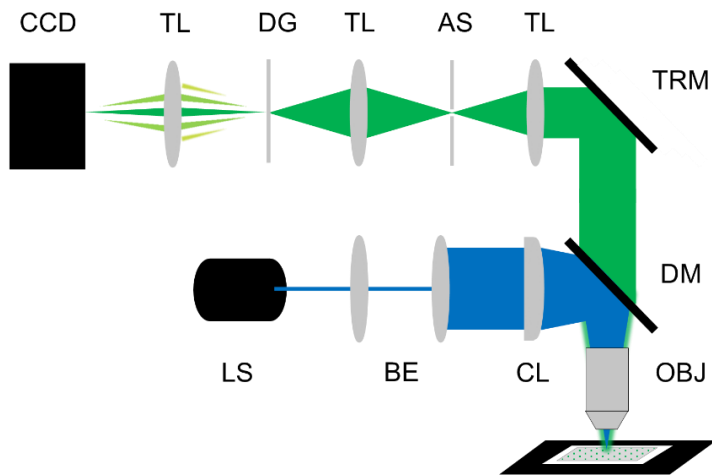
Figure 3: LS: Laser Source, BE: Beam Expander (5x), CL: Cylindrical Lens, DM: Dichroic Mirror, OBJ: Objective (20x, 0.50 NA) , TRM: Total Reflection Mirror, TL: Tube Lenses, AS: Adjustable Slit, DG: diffraction Grating, CCD: Flea 3 Camera.

grating (DG, Throlabs, Newton, NJ). The 25 mm x 25 mm grating has 300 groves/mm with a groove angle of 17.5°. The diffracted light expands to a 50 mm lens, where the light is focused onto a monochromatic Flea 3 camera (CCD, Point Grey, FLIR, Wilsonville, OR, USA). The camera was aligned with the m = 1, 0, and -1 diffraction orders. The multiple diffraction orders allow for maximum pixel intensity with adequate separation of light and visualization of the non-diffracted light (m = 0) as a reference.

II.   *Slide Preparation and Image Acquisition*

The system and image acquisition procedures were calibrated using FluoSpheres polystyrene microspheres with a 15 µm diameter (Invitrogen, Eugene, OR). The yellow-green microspheres (505 nm/515 nm) were used to interpret shorter emission wavelengths and model the emission characteristics of the lymphocytes, which have green emission close to 525 nm. The crimson microspheres (625 nm/645 nm) were used to interpret longer wavelengths and model the emission of the granulocytes, which fluoresce in the red-orange region with a wavelength of 650 nm. Two slides for each color of microsphere were prepared using 10 µL of microspheres diluted in a 1:100 solution on a white 25 x 75 x 1 mm Superfrost plus micro slides (VWR, Radnor, PA) and covered with 22 x 22 mm No. 2 cover glass. Images of the microspheres were acquired with the image-based spectrometer optical setup using the 20x objective. For the yellow-green microspheres, the camera parameters were set to a gain of 0 dB and an exposure time of 75 ms. For the crimson microspheres, the camera parameters were set to a gain of 20 dB and an exposure time of 150 ms. Both microsphere slides were imaged with a laser power of 8.85 mW at the sample. Single, stationary images were acquired for both colored slides. Videos of a

6

manually translated yellow-green microsphere slide were acquired over a period of 10,000 ms using the same camera settings and laser power.

Images of whole blood stained with the AO fluorescent dye were acquired similarly to the microspheres. A 20 µg mL^{-1} AO solution was prepared using acridine orange hemi(zinc chloride) salt (Sigma-Aldrich, St. Louis, MO) in deionized water. Whole blood was collected via finger stick (IRB # 13-06-759) and stained with the AO solution at a 1:1 ratio. The slide was prepared with Superfrost plus micro slides, 10 µL of the AO-stained blood, and 22 x 22 mm No. 2 cover glass. Using the 20x objective, the camera parameters were set to a gain of 25 dB and an exposure time of 350 ms. The laser power at the sample was 8.85 mW. Images were acquired after a 10 minute period.

III. *Spectral Extraction Algorithm*

A MATLAB algorithm, flow chart in **Figure 4**, was designed to analyze the spectral data within the images acquired using the image-based spectrometer. The algorithm first rotated each image 270 degrees counter-clockwise using the *imrotate*(image, degrees) function to orient the spectral information in the way visible light wavelengths expand from violet to red light. A high binary threshold of 70 was applied to the rotated image to distinguish between scattered light and light native to the original objects. The objects were assigned a pixel value of 1, and the background and other pixel contributions were assigned a pixel value of 0. These pixel values limited by the binary threshold were only used during the watershed segmentation, described next. The threshold-limited pixel values were smoothed using the open and close functions to create a more circular appearance of each object. A Fourier disk function with a radius of 5 pixels was applied to the image as a whole to serve as a filter during the watershed segmentation— *watershed*(filter). This disk filter acted as boundary condition for the segmentation of each of the objects in the image. The watershed segmentation was performed to separate particles that were merged during the binary image thresholding. The watershed separation technique is based on the peaks and valleys of the intensity in the image. The borders of the segmented particles calculated using the watershed and disk functions were used to determine the location of each centroid in the image using the *regionprops*(image, 'Centroid') function. The output of the centroid location function was the x-y pixel coordinates of the center of each object in the image.

The original images underwent a new, lower threshold with a value of one to eliminate noise produced by the image sensor. The intensity changes across the entire x-axis of the image represented the emission profile of the object. The fluorescence emission profile was collected using the y-axis location of each centroid detected during the watershed segmentation. The y-axis location of the centroid was the central row of the object. This value was used to evaluate the emission profiles of each object. The object diameter for each centroid was determined using the *regionprops*(image,'MinorAxisLength') function. The diameter value was used to calculate how many rows needed to be analyzed to process the entire object. The maximum intensity value of each line across the image was determined using the *max*(row number) function. The single line profile's pixel values were divided by the corresponding maxima to scale each row from 0 to 1 separately in order to normalize images with different fluorescence intensities. The scaled values for each row across an object were stored in a temporary array, where a mean for each column was calculated to get an average profile across total length of the object. This average intensity profile was plotted using the x-pixel locations, corresponding to emission wavelength, vs. scaled pixel values, corresponding to the fluorescence intensity. Each curve was sub-plotted on the same figure to compare the curves for each object in the same image. After, a high-order line-of-best-fit curve was developed for each line profile to quantify the emission profile and changes between each object. The mean of the polynomial order coefficient values for each line profile was saved in a separate array. The total number of objects processed in the images was determined based on the total length of the best-fit curve array using the *length*(array) function. Using this information, the spectra of individual objects were distinguished based on the mean value of each best-fit curve and stored for future studies that will apply classification methods to differentiate objects into different colorimetric groups.

The video file collected of the manually translated beads was broken down into individual frames. These frames were processed using the same methods as the stationary images with the addition of the *unique*(centroid location array) function. This additional function allowed for the detection of previously processed objects that appeared in preceding images. All centroid x-y locations were stored in a total centroid array to assure each unique value would not be repeatedly processed. If the object appeared twice in two separate images, the object was only

processed in the first image. This did not inhibit the processing of new objects in the following images.
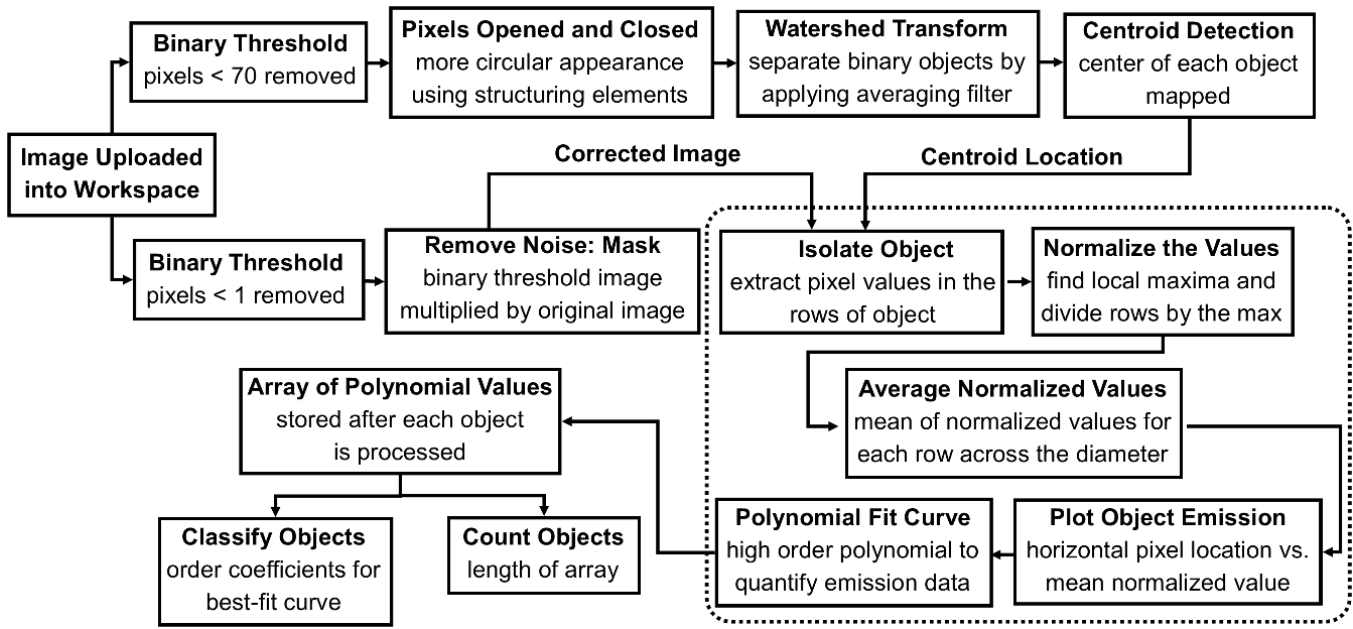

Figure 4: A flow chart describing the flow of commands applied to a single image to isolate the spectral information for each object in an image.

Results

I. Image Acquisition and Diffraction Order Effect on the Emission Profile

The early iteration of the image-based spectrometer system isolated the $m = 1$, 0, and -1 diffraction orders when focused onto the CCD by the 50 mm tube lens. The three diffraction orders were imaged within one field of view, as demonstrated in **Figure 5 (left)**. These object emission intensities were dependent on the diffraction orders, where the $m = 0$ order had the highest pixel intensity due to the absence of diffraction. The $m = -1$ and 1 orders exhibited a significant drop in pixel intensity, especially in the $m = 1$ order. An intensity-based emission profile across the image characterized these changes as three distinct peaks along the line, demonstrated by the yellow line in **Figure 5 (right**) and related to the emission profile on the left. The change in intensity was related to the principles of the diffraction grating, where the diffraction of the light by the grating system diminishes pixel intensity for the respective diffractive order as the light was separated. This trend continued as the orders grew in magnitude with the

highest visible orders (m = 1 and -1) being the most successful in separating the wavelengths while providing high fluorescence intensity. The m = -1 order had the highest intensity when compared to the m = 1 emission profile, so it was most attractive for further processing.
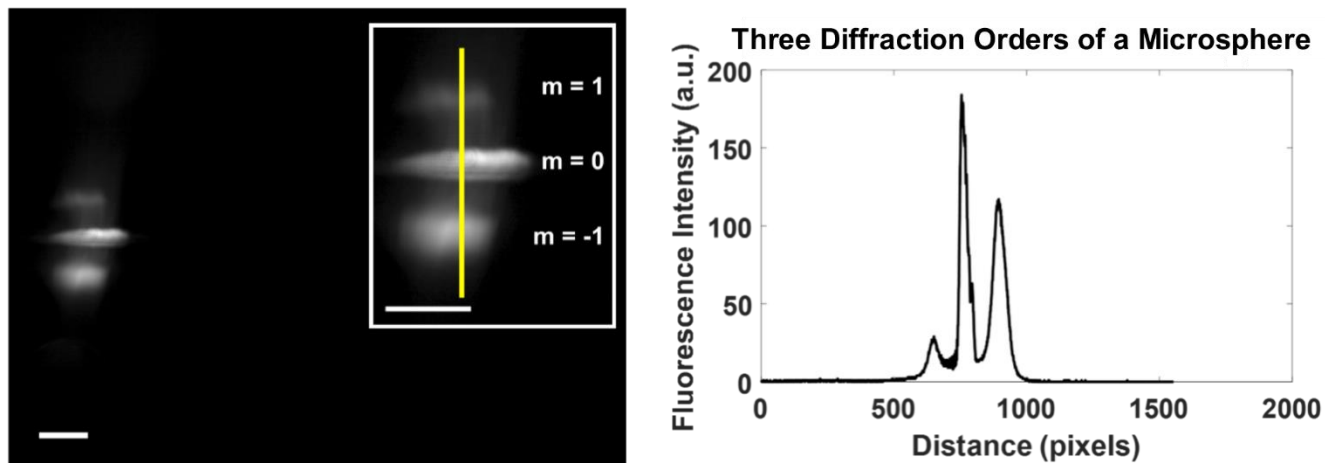

Figure 5: (left) A spectral image of a green microsphere demonstrating three diffractive orders (inset). (right) The intensity profile of the yellow line in the inset. Scale bar 20 µm.

II.   *Image Post-processing to Isolate Individual Emission Profiles*

The images of the stationary microsphere slides were cropped to isolate the m = -1 diffraction order. The cropped images were reduced from 2080 x 1552 pixel images to 2080 x 198 pixel images. The cropped yellow-green and crimson microsphere images were loaded into the MATLAB algorithm and underwent the watershed segmentation to distinguish objects and develop corresponding emission profiles, **Figure 6**. The "original image" was the cropped image of the isolated m = -1 diffraction order. This image underwent the watershed segmentation to distinguish emission profiles that were close together. The segmentation was based on the intensity changes across an image, while looking for peaks and valleys corresponding to object boundaries using the Distance Transform. The center of each object was effectively determined using the boundaries of the watershed segmentation. The emission profiles of each object isolated in an image were created as a result of the object segmentation and intensity processing.
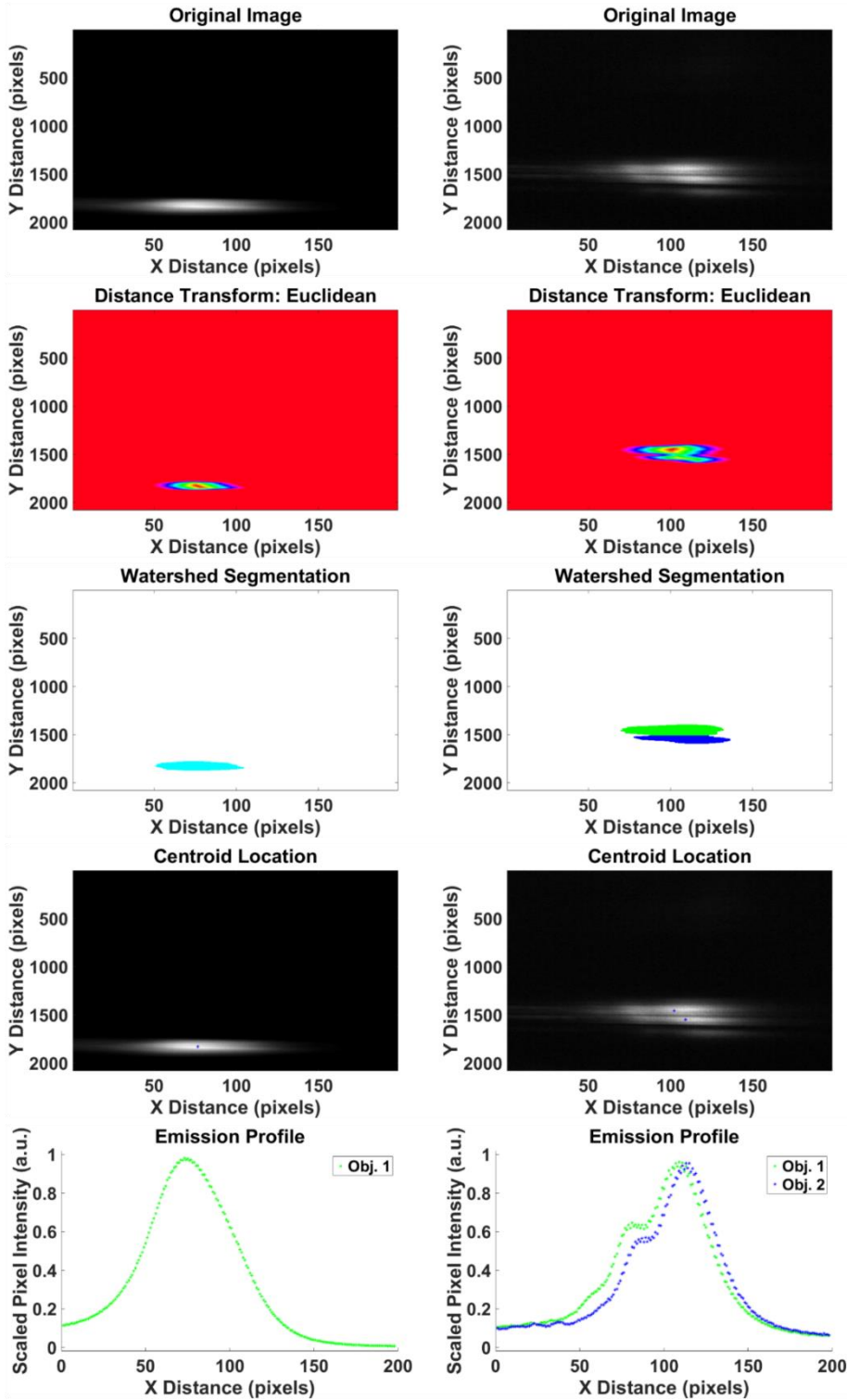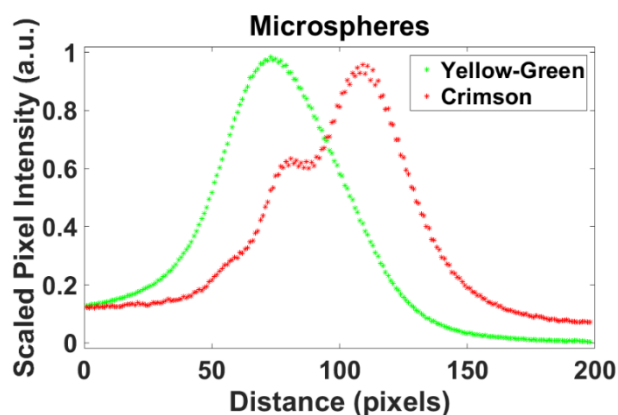
Figure 6: The image processing was done using a custom MATLAB algorithm. The original image underwent a watershed segmentation using a Euclidean distance transform to create the object boundaries. The object boundaries were used to locate the centroid location for each object in the image. The emission profiles were created based on the intensity changes across the image and its center location.

III.   Spectral Data Extracted from Individual Objects

The emission profiles of the microspheres were processed first to understand the emission wavelength positions across the image. The scaled pixel intensities for both microspheres were plotted against the pixel distance (0-198 pix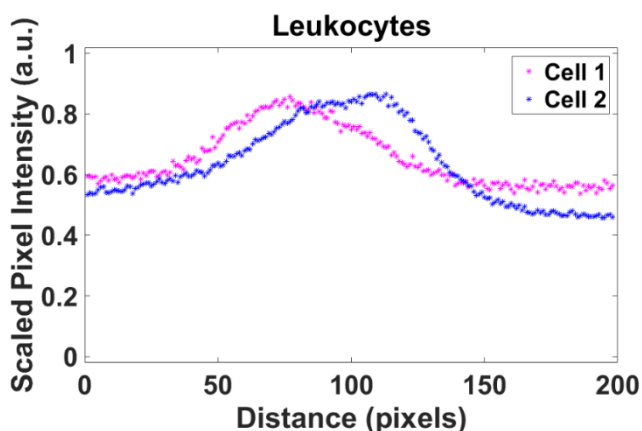els) in the image, **Figure 7**. The approximate pixel distance across the line (x-axis) would relate to the wavelengths associated with the emission profile provided by the microsphere manufacturer. A pixel distance of 75 would relate to the peak

Figure 7: The spectral profile of the yellow-green and crimson microspheres. The pixel intensity is scaled from 0-1 due to the camera setting differences between the images.

emission of the yellow-green microsphere at 515 nm, and a pixel distance of 125 would relate to the peak emission of the crimson microspheres at 645 nm. The yellow-green (515 nm) and crimson (645 nm) microspheres exhibited distinct separation in colorimetric emission with a peak-to-peak difference of 36 pixels, which is related to the 130 nm peak emission difference.

Leukocytes stained with AO were also cropped using the same function as the microspheres. The noise in the AO-stained images was significantly higher than the microsphere images. The average pixel intensity of the leukocytes was also much lower, thus requiring higher gain and exposure time settings. Two AO stained leukocytes exhibited distinct emission profiles and peaks across different wavelengths, **Figure 8**. This could be due to variations in the staining method (incubation


Figure 8: The emission profile of two leukocytes stained with AO. The distance in pixels represents a change in wavelength emission.

period or AO concentration) affecting the emissions or in cellular content relating to different leukocyte subtypes. Each processed cell demonstrated a profile within the pixel range characterized by the yellow-green and crimson microspheres, thus further supporting the use of

these microspheres to calibration the system. The noise contributed to poor quality of the emission curves of the leukocytes, where the scaled curve minimum was approximately 0.5 with a maximum for each cell less than the maximum of one.

IV. Isolation of Unique Objects from Video Frames of a Translated Slide

The frames that were isolated from the video of the translated yellow-green microsphere slide were processed using the same MATLAB algorithm. While the video was acquired, a new frame was collected every 10 ms. The manual translation speed is slower than the frame acquisition rate, so the same objects appeared in multiple frames. The unique centroid detection was effective at preventing the processing of the same object twice. The video frames were not cropped to isolate the m = -1 diffraction order before the image processing began, like the stationary image. Instead, the centroid detection used the m = 0 order to detect the number of objects in an image, **Figure 9**. After the centroids were detected and repeat values were removed, the m = -1 order was isolated to create the emission profiles for each unique object in the image.
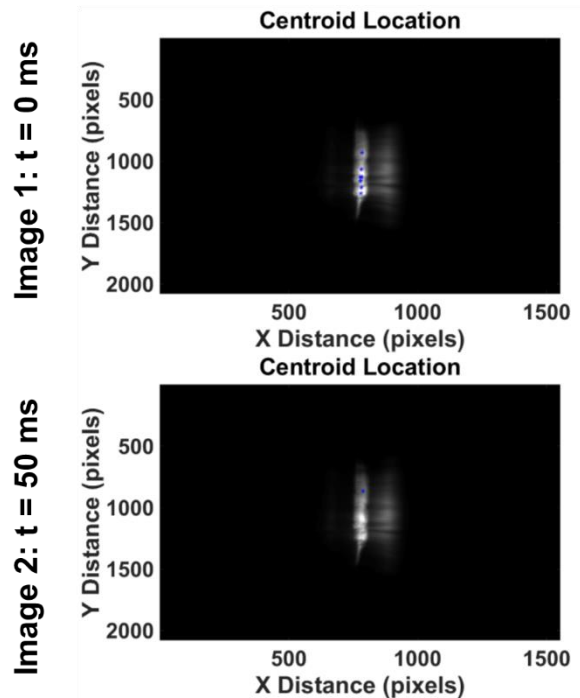
Figure 9: The video frames of the translated slide analyzed to distinguish unique and repeating objects in consecutive frames.

Discussion

The custom MATLAB algorithm successfully isolated the emission spectra of stationary microspheres and AO stained leukocytes produced by the image-based spectrometer system. The algorithm was also able to distinguish moving objects that had been previously analyzed. The stationary images were cropped to isolate the diffraction order with the highest pixel intensity. The emission profiles extracted across the cropped microsphere and leukocyte images were within the same 0-198 pixel range. This suggests that the isolated m = -1 diffraction order's pixel width corresponded to the visible color wavelengths within the microsphere and AO emission ranges of 500-700 nm. Additionally, the emission profile peaks of each AO stained

leukocyte, **Figure 9**, co-aligned with the peaks of the microsphere emission profiles, **Figure 8**, thus confirming the microspheres as a system and algorithm calibration tool. The m = -1 diffraction order was effectively isolated by cropping the image; however, the cropping eliminates the value of a full field of view of 2080 x 1552 pixels. Future iterations of the system will need increased magnification to acquire data from only one diffraction order. The single diffraction order will possess a more complete spectrum across 1552 pixels, which will allow for more detailed curve data for later spectrum classification processes.

The two leukocyte emission profiles, **Figure 8**, did exhibit colorimetric differences characterized by slight variations in their peaks. For Cell 1, the peak lies on the left indicating that the cell had more dominant green fluorescence, while Cell 2 had a peak shifted to the right indicating that the cell had slightly more red fluorescence. Initially, this could suggest that Cell 1 is a lymphocyte and Cell 2 is a granulocyte; however, many factors could have contributed to this difference, such as incubation period, AO staining concentration, and cellular content. Specifically, in this study, the cells were known to be imaged at different incubation periods. Therefore, highly controlled staining methods and large number of cells need to be measured in order to distinguish different leukocyte subtypes and classify a distinct spectral pattern as a specific cell type.

The video data for the translated yellow-green microsphere slide was processed with an early understanding of the way the CCD processes the moving objects. The frames were acquired at a much faster rate than the manual translation stage was moved. Image acquisition parameters could be improved to limit the number of frames that are identical, because the same objects appeared in up to 40 consecutive images with no new objects for five images. The emission profiles for the yellow-green microspheres were similar to the stationary yellow-green microsphere curves. Therefore, the translation of the microspheres did not affect the quality or peak pixel distance for the emission profile of the microspheres. Additional methods could be employed to assure that objects in the video frames are not missed or counted more than once. MATLAB has object tracking functions, which could be utilized in addition to the centroid location detection. These methods would be most pertinent when the spectrum are used to generate a total object count.

Conclusions

We have demonstrated the ability to extract spectral information from data acquired from the image-based spectrometer of microspheres, as a control, and AO stained leukocytes. We determined that the spectral information from yellow-green and crimson microspheres could be used to represent the wavelength range of AO stained leukocytes, thus providing a calibration tool. Also, preliminary spectral information was extracted from linearly translated yellow-green microspheres. The majority of images acquired for this project were still frame images of a stationary slide. However, this stationary image acquisition procedure limited the number of object emission profiles collected in a single image. The spectral information from the video frames are in the early stages of isolating unique spectra across numerous images; however, it demonstrates the feasibility of collecting data for a larger number of objects. The image acquisition and image processing techniques presented here will be used to extract and organize spectral data for further analysis. We will identify each subtype of cells using standard classification methods and to determine any time-dependent emission changes.

Acknowledgements

References

1. Von Bertalanffy L, Masin M, Masin F. A new and rapid method for diagnosis of vaginal and cervical cancer by fluorescence microscopy. *Cancer* 1958; 11: 873-887.
2. Bertalanffy FD. Diagnostic Reliability of the Acridine Orange Fluorescence Microscope Method for Cytodiagnosis of Cancer. *Cancer Research* 1961; 21: 422-426.
3. Lauer BA, Reller LB, Mirrett S. Comparison of Acridine Orange and Gram Stains for Detection of Microorganisms in Cerebrospinal Fluid and Other Clinical Specimens. *Journal of Clinical Microbiology* 1981; 14:201-205.
4. Pierzynska-Mach A, Janowski PA, Dobrucki JW. Evaluation of Acridine Orange, LysoTracker Red, and Quinacrine as Fluorescent Probes for Long-Term Tracking of Acidic Vesicles. *Cytometry* 2014; 85A: 729-737.
5. Bhakdi SC, Sratongno P, Pattamawan C, et al. Re- evaluating Acridine Orange for Rapid Flow Cytometric Enumeration of Parasitemia in Malaria-infected Rodents. *Cytometry* 2007; 71A: 662-667.

6. Von Bertalanffy L, Masin M, Masin F, Kaplan L. Detection of Gynecological Cancer, Use of Fluorescence Microscopy to Show Nucleic Acids in Malignant Growth. *California Medicine* 1957; 87(4): 248-251.

7. Majors CE, Pawlowski M, Tkaczyk T, Richards-Kortum R. Imaging Based System for Performing a White Blood Cell Count and Partial Differential at the Point of Care. *Biomedical Optics Congress* 2016.

8. Powless AJ, Conley, RJ, Freeman KA, Muldoon TJ. Considerations for point-of-care diagnostics: evaluation of acridine orange staining and postprocessing methods for a three-part leukocyte differential test. *Journal of Biomedical Optics*. 2017. 22 (3): 035001.

9. Traganos F, Darzynkiewicz Z. Lysosomal Proton Pump Activity: Supravital Cell Staining with Acridine Orange Differentiates Leukocyte Subpopulations. *Methods in Cell Biology* 1994; 41: 185-194.

10. Jahanmehr SAH, Hyde K, Geary CG, Cinkotai KI, Maciver JE. Simple technique for fluorescence staining of blood cells with acridine orange. *Journal of Clinical Pathology* 1987; 40: 926-929.

11. Gerstner AO et al. Comparison of immunophenotyping by slide-based cytometry and by flow cytometry. *Journal of Immunological Methods* 2006; 311(1-2): 130-138.

12. Houwen B. The Differential Cell Count. *Laboratory Hematology* 2001; 7: 89-100.

13. Forcucci A, Pawlowski ME, Majors C, Richards-Kortum R, Tkaczyk TS. All-plastic, miniature, digital fluorescence microscope for three part white blood cell differential measurements at point of care. *Biomedical Optics Express* 2015; 6(11): 4433-4446.

14. Palmer C, Loewn E. (2005). *Diffraction Grating Handbook, sixth edition*. Rochester, New York: Newport Corporation.

15. Loewen EG, Popov E. (1997). *Diffraction Gratings and Applications*. New York, New York: Marcel Dekker, Inc.